J Neurophysiol 119: 389–400, 2018.
First published October 18, 2017; doi:10.1152/jn.00872.2016.

RESEARCH ARTICLE | *Biology of Neuroengineering Interfaces*

Spatiotemporal characteristics of retinal response to network-mediated photovoltaic stimulation

Elton Ho,[2]* Richard Smith,[1]* Georges Goetz,[2] Xin Lei,[3] Ludwig Galambos,[3] Theodore I. Kamins,[3] James Harris,[3] Keith Mathieson,[5] Daniel Palanker,[2,4] and Alexander Sher[1]

[1]*Santa Cruz Institute for Particle Physics, University of California, Santa Cruz, California;* [2]*Hansen Experimental Physics Laboratory, Stanford University, Stanford, California;* [3]*Department of Electrical Engineering, Stanford University, Stanford, California;* [4]*Department of Ophthalmology, Stanford University, Stanford, California; and* [5]*Institute of Photonics, University of Strathclyde, Glasgow, Scotland, United Kingdom*

Submitted 9 November 2016; accepted in final form 13 October 2017

Ho E, Smith R, Goetz G, Lei X, Galambos L, Kamins TI, Harris J, Mathieson K, Palanker D, Sher A. Spatiotemporal characteristics of retinal response to network-mediated photovoltaic stimulation. *J Neurophysiol* 119: 389–400, 2018. First published October 18, 2017; doi:10.1152/jn.00872.2016.—Subretinal prostheses aim at restoring sight to patients blinded by photoreceptor degeneration using electrical activation of the surviving inner retinal neurons. Today, such implants deliver visual information with low-frequency stimulation, resulting in discontinuous visual percepts. We measured retinal responses to complex visual stimuli delivered at video rate via a photovoltaic subretinal implant and by visible light. Using a multielectrode array to record from retinal ganglion cells (RGCs) in the healthy and degenerated rat retina ex vivo, we estimated their spatiotemporal properties from the spike-triggered average responses to photovoltaic binary white noise stimulus with 70-μm pixel size at 20-Hz frame rate. The average photovoltaic receptive field size was 194 ± 3 μm (mean $\pm$ SE), similar to that of visual responses (221 ± 4 μm), but response latency was significantly shorter with photovoltaic stimulation. Both visual and photovoltaic receptive fields had an opposing center-surround structure. In the healthy retina, ON RGCs had photovoltaic OFF responses, and vice versa. This reversal is consistent with depolarization of photoreceptors by electrical pulses, as opposed to their hyperpolarization under increasing light, although alternative mechanisms cannot be excluded. In degenerate retina, both ON and OFF photovoltaic responses were observed, but in the absence of visual responses, it is not clear what functional RGC types they correspond to. Degenerate retina maintained the antagonistic center-surround organization of receptive fields. These fast and spatially localized network-mediated ON and OFF responses to subretinal stimulation via photovoltaic pixels with local return electrodes raise confidence in the possibility of providing more functional prosthetic vision.

NEW & NOTEWORTHY Retinal prostheses currently in clinical use have struggled to deliver visual information at naturalistic frequencies, resulting in discontinuous percepts. We demonstrate modulation of the retinal ganglion cells (RGC) activity using complex spatiotemporal stimuli delivered via subretinal photovoltaic implant at 20 Hz in healthy and in degenerate retina. RGCs exhibit fast and localized ON and OFF network-mediated responses, with antagonistic center-surround organization of their receptive fields.

brain-machine interface; electrical stimulation; electrophysiology; neural prosthesis; retinal ganglion cells; retinal prosthesis

INTRODUCTION

Retinal degenerative diseases, such as retinitis pigmentosa and age-related macular degeneration, cause a gradual loss of photoreceptors in millions of patients worldwide and are the leading cause of incurable blindness in the developed world (Smith et al. 2001). However, most of the inner retinal neurons survive in these diseases, despite some changes in the wiring of the retinal circuitry (Jones and Marc 2005; Marc and Jones 2003). Retinal prostheses aim at restoring sight by reintroducing information into the visual system using electrical stimulation of the remaining retinal neurons (Goetz and Palanker 2016; Yue et al. 2016). Epiretinal prosthetic devices primarily target the retinal ganglion cells (RGCs), spiking neurons that represent the output cascade of the retinal signal processing. A major difficulty with this approach is that bundles of axons from distant RGCs passing under the epiretinal electrodes are also stimulated, which results in arcuate percepts distorting the retinotopic map of the image (Nanduri et al. 2012). Avoiding this effect during the use of submillisecond pulses is very difficult because stimulation thresholds of the axons in the nerve fiber layer are similar to those of RGCs. Such a distortion can be avoided by applying much longer (~25 ms) pulses (Weitz et al. 2015), which are more likely to activate inner retinal neurons while avoiding direct ganglion cell activation, because these nonspiking neurons in the inner nuclear layer have significantly lower stimulation thresholds at long pulse durations than RGCs do (Boinagrov et al. 2014; Freeman et al. 2010). Subretinal implants are closer to the inner nuclear layer and activate these neurons (Lorach et al. 2015b; Mathieson et al. 2012) with lower thresholds than the ganglion cells (Boinagrov et al. 2014), thereby reducing the likelihood of axonal activation. Both epiretinal (ARGUS II, Second Sight; and IRIS 2, Pixium Vision) and subretinal (Alpha IMS, Retina Implant) prostheses currently approved for clinical use require a transscleral cable for transfer of signals and/or power to the stimulating array (Ho et al. 2015; Humayun et al. 2012; Stingl et al.

* E. Ho and R. Smith contributed equally to this work.

Address for reprint requests and other correspondence: A. Sher, Santa Cruz Institute for Particle Physics, Univ. of California, Santa Cruz, CA 95064 (e-mail: sashake3@ucsc.edu).

2013b). This requirement leads to difficult surgical procedures and increases probability of postimplantation complications.

We therefore developed a prosthetic system where both power and information are delivered optically to a subretinal array of photovoltaic pixels (Mathieson et al. 2012; Palanker et al. 2005). A video stream is projected onto the implant from video goggles using pulsed near-infrared light (NIR) (Goetz et al. 2013). The implant converts light pulses into charge-balanced pulses of electric current in each pixel (Boinagrov et al. 2016), which stimulate the nearby inner retinal neurons. The use of NIR light (wavelength, 880–915 nm) avoids both photophobic and phototoxic effects associated with intense illumination (Lorach et al. 2016).

We demonstrated previously that photovoltaic subretinal stimulation can elicit retinal and cortical responses in healthy animals [Long-Evans (LE) rats] and in animals with degenerate retina [Royal College of Surgeons (RCS) rats] at safe illumination levels (Lorach et al. 2015a, 2015b; Mathieson et al. 2012). We characterized the response properties of RGCs using high-frequency (20 Hz) stimulation, whereas the amplitude envelope of this carrier frequency was modulated at a lower frequency (1 Hz), resulting in slow full-field changes in intensity. Using this paradigm, we assessed contrast sensitivity and spatial resolution with alternating gratings (Goetz et al. 2015; Lorach et al. 2015b). We found that only the first few stimulation pulses following the increase in intensity elicited an increase in spiking of the RGCs, demonstrating that the network-mediated response to subretinal electrical stimulation exhibits flicker fusion and adaptation to static images (Goetz et al. 2015; Lorach et al. 2015b). These observations suggested that flicker-fused prosthetic vision might be possible, even though clinical implants currently use a much lower frequency ($<$7 Hz) in patients (Stingl et al. 2013a). It remained unknown, however, whether RGCs could respond to complex spatiotemporal photovoltaic stimulation at naturalistic frequencies and how their response properties would compare with the normal visual responses to such stimuli.

The goal of this study was to investigate RGC responses to complex spatiotemporal electrical activation patterns and to compare them with natural visual responses in the healthy retina. We used a custom-made transparent extracellular microelectrode array (MEA) (Litke et al. 2004) and spatiotemporal binary white noise to jointly characterize the spatial and temporal response properties of RGCs to photovoltaic subretinal and visual stimulation in the healthy (LE) and degenerate (RCS) rat retina. Spike-triggered average (STA) responses of RGCs to white noise stimulation (Chichilnisky 2001) have been extensively used to measure response properties of the healthy retina (Chander and Chichilnisky 2001; Devries and Baylor 1997; Field et al. 2007, 2010; Sher and DeVries 2012). Measurements of the spatial receptive fields and response dynamics of individual RGCs enable their classification into functional types, representing parallel retinal pathways that extract various features of the visual scene. Two major RGC types are ON- and OFF-center cells that respond to the onset and offset of light, respectively, in their receptive field centers and have opposing wider surrounds.

We show that the hallmark RGC visual properties, such as fast response time, spatially localized receptive field, and opposing surround, are present with subretinal photovoltaic stimulation of both healthy and degenerated retina. This indicates that spatial and temporal characteristics of prosthetic vision, mediated by a subretinal photovoltaic array, may closely resemble the normal visual responses.

METHODS

Implant fabrication. Photovoltaic arrays were manufactured on silicon-on-insulator wafers using a six-mask lithographic process. Different versions of the devices were fabricated with either two or three diodes in series per pixel, with anodic-first polarity on active electrode. The arrays consisted of 70-μm-wide pixels, separated by 5-μm trenches (Fig. 1, *A–C*). Details of the fabrication process were described previously for pixels of the opposite wiring polarity (Wang et al. 2012).

Electrophysiological recording. Retinal responses were recorded from four adult healthy Long-Evans [LE; ages postnatal day 60 (p60) to p100] and seven degenerate Royal College of Surgeons (RCS) rats (age p120 to p360), all of which were kept in accordance with the institutional guidelines and conformed to the guidelines of the Asso-

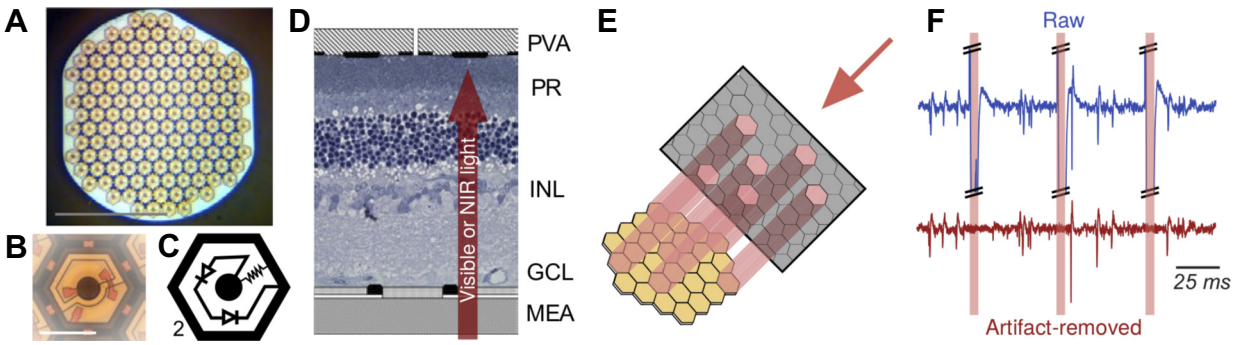

Fig. 1. Photovoltaic array and experimental setup. *A*: a single module of the photovoltaic prosthesis is composed of 70-μm-wide pixels separated by 5-μm trenches arranged in a 1-mm-wide hexagonal pattern, with the adjacent rows separated by 65 μm. *B*: close-up photograph of a 2-diode, 70-μm-wide pixel. *C*: wiring diagram: each pixel consists of 2 (shown) or 3 photodiodes connected in series between the central active (*1*) and surrounding return (*2*) electrode. *D*: schematic representation of a healthy rat retina sandwiched between a transparent MEA, which records from the ganglion cell layer (GCL) and the photovoltaic array (PVA). Visible light stimulates the photoreceptors (PR), while much brighter pulsed NIR (880–915 nm) illumination generates biphasic pulses of electric current flowing through the tissue between the active and return electrodes of photovoltaic pixels. *E*: schematic representation of stimulus patterning. An LCD screen modulates the incoming pulsed laser illumination. A white noise stimulus frame is shown. Each pixel in the image is aligned with a pixel on the implant. *F*: example voltage trace from 1 of the 512 individual electrodes, before and after artifact removal. Each electrode detects action potentials of multiple cells along with electrical artifacts from the activation of the photodiodes. These artifacts are removed by *1*) blanking a short period (~8 ms), during which spikes are not recovered, and *2*) subtracting a difference of Gaussian function from the raw trace. The parameters of the function are fitted to the data for each artifact on each electrode separately.

ciation for Research in Vision and Ophthalmology (ARVO) Statement for the Use of Animals in Ophthalmic and Vision Research. The University of California Santa Cruz Institutional Animal Care and Use Committee approved all experimental procedures used for this research. Only one retinal recording was obtained from each rat. Retinal tissue was mounted according to previously described procedures (Goetz et al. 2015). In summary, the eyes were enucleated from a euthanized (390 mg/kg pentobarbital sodium, 50 mg/ml phenytoin sodium) rat. After vitrectomy, an ~3-mm × 3-mm piece of the isolated retina was placed ganglion cell side down on the 512-electrode MEA (Litke et al. 2004). The retina was constantly perfused with Ames' medium at 29.4°C and bubbled with a mixture of 95% O_2 and 5% CO_2. The photovoltaic array was placed carefully on top of the retina and pressed onto the retina and underlying MEA with a 100-μm cell size nylon mesh. The voltages on the 512 electrodes were amplified and digitized with 20-kHz sampling frequency using a custom-made readout electronics and data acquisition system (Litke et al. 2004). The stimulation was delivered to the photoreceptors or the photodiode array from below through the transparent MEA and the retina (Fig. 1*D*). In a typical preparation, RGCs had stable responses to stimulation for several hours.

Retinal stimulation. Light sourced from either an NIR (880 nm) diode laser for photovoltaic stimulation (4-ms pulses at 20 Hz, 9 mW/mm^2 peak power) or a yellow (591 nm) LED for visual stimulation (continuous illumination) was coupled into the same optical path. Images were formed by an amplitude modulation in a transmissive LCD screen (Holoeye HEO-0017), as described previously (Goetz et al. 2015; Lorach et al. 2015a). The 8-bit LCD panel had a 60-Hz native frame rate, 1,024 × 768 resolution with a square pixel layout, and a white-to-black intensity ratio of 10,000:1 at 520 nm and 200:1 at 880 nm. The pixel size projected onto the retina was 6 μm.

A spatiotemporal binary white noise stimulus was used to characterize spatiotemporal response properties of the RGCs (Chichilnisky 2001). Each pixel in each frame had a 50% chance to be white or black, independently from others and from frame to frame. The white noise for visual stimulation was shown at 30-Hz frame rate and consisted of square pixels of 60 μm in size focused on the photoreceptor layer. The white noise for photovoltaic stimulation had 20-Hz frame rate and consisted of hexagonal pixels that were matched in size and location to the 70-μm hexagonal pixels of the implant, resulting in each hexagonal image pixel illuminating 1 pixel on the implant (Fig. 1*E*). The duration of each white noise stimulus recording was 30 min. Photovoltaic stimulation was applied at a low rate to minimize problems caused by the electrical artifact elicited on the recording electrodes by the stimulation pulses. The lower frame rate resulted in lower temporal resolution of the RGC response to photovoltaic compared with visual stimulation.

Full-field flashes were also used to measure RGC responses to photovoltaic stimulation. The train of 4-ms NIR pulses repeated at 20 Hz was modulated in intensity at 1-Hz frequency (Goetz et al. 2015). Each alternate full-field image was presented for 500 ms and had an irradiance level of 10 mW/mm^2, whereas the other full-field image was dark, resulting in +100% and −100% contrast transitions. The contrast steps were presented a total of $n = 100$ times.

Neuron finding. Photovoltaic stimulation produces a large electrical artifact unique to each of the 512 recording electrodes and different for each frame of the white noise movie. We fitted the artifact using a difference of two Gaussians. The fitted function was then subtracted from the raw voltage trace. This procedure was repeated for each artifact on each of the individual electrodes. The artifact was too large during the first 8.25 ms after the laser pulse for this procedure to work; therefore, we replaced this 8.25-ms period with randomly generated noise that matched the noise level of the electrode in question. As a result, any action potentials that occurred within 8.25 ms from the start of the laser pulse were lost. We expect that the omission of some of the elicited spikes might result in an underestimation of the strength of the RGC response. Figure 1*F* shows an example voltage trace from one of the electrodes before and after the subtraction. The artifact-subtracted raw data were then used to find and sort action potentials (spikes). Spikes were defined as an event where the negative voltage deflection amplitude exceeded three times the root-mean-squared noise on each electrode. Custom-made software was used to perform spike sorting as described previously (Field et al. 2010; Goetz et al. 2015; Litke et al. 2004). In short, to identify spikes of individual RGCs, all waveforms underwent dimensionality reduction by noise-whitened principal component analysis, and spike trains of putative neurons were obtained by expectation-maximization clustering. For each candidate neuron, an estimate of the fraction of spikes coming from other neurons ("contaminating" spikes) was obtained from the number of refractory period violations in the spike train. We excluded from our analysis contaminated neurons that had over 10% of their spikes coming from another cell. Furthermore, we excluded from the analysis putative neurons that had abnormal electrophysiological images (EIs) (e.g., EIs showing backward propagation of the axonal signal). Each of these selection criteria removed less than 10% of the cells with good responses to the stimulus as defined in the next subsection. The electrophysiological image is the average electrical signal measured on all of the recording electrodes within 10 ms of the RGC spike and typically shows both soma location and the axonal trajectory of the RGC (Li et al. 2015; Petrusca et al. 2007).

Spike sorting was performed separately for retinal responses to each stimulus. We used each neuron's unique EIs to match the individual cells across multiple stimulus conditions (Li et al. 2015; Sher and DeVries 2012). This match was performed between RGCs identified in the visual and photovoltaic stimulation runs in each LE retina and between the RGCs identified in the visual and photovoltaic stimulation of the retina in the pharmacology experiment. For these experiments, only the cells that were successfully matched between the stimulation conditions were retained for analysis. The fraction of RGCs with significant photovoltaic responses (see below) that were matched to the visually responding cells varied from 90% to 50% between preparations.

Characterization of the RGC responses. Each cell's spatiotemporal response properties was estimated by calculating the STA response of each RGC to the white noise stimulus (Chichilnisky 2001). Short white noise movies (typically 20 frames) that preceded each of the detected spikes of an RGC are averaged over the recording to obtain the STA of the RGC (Fig. 2*A*). The spatial sensitivity profile of the RGC (receptive field) corresponds to the STA regions with significant deviations from the average gray level. We quantified the spatial extent of the receptive field by the 1-σ contour of the two-dimensional Gaussian fitted to the STA frame with the largest deviation from gray level (Fig. 2*B*). The receptive field size is estimated as the diameter of a circle with the area equivalent to that of the ellipse. The time course shows the STA intensity within the receptive field as a function of time preceding the spike (Fig. 2*B*). In a fully linear system, convolution of the time course with the full-field step in illumination provides the predicted response of the cell to such a step. Therefore, the sign of the first peak preceding the spike in the time course determines if the RGC increases its spiking rate in response to the ON- or OFF-set of light (Chichilnisky and Kalmar 2002). We used the time courses of individual RGCs to distinguish between the two major RGC types: ON- and OFF-center (Chichilnisky and Kalmar 2002; Sher and DeVries 2012). STAs of example ON- and OFF-center RGCs are shown in Fig. 2*B*. The spatiotemporal white noise is not well suited for classifying ON-OFF cells. ON and OFF parts of an ON-OFF receptive field would be averaged by the STA resulting in either *1*) no response if they are matched exactly and cancel each other, or producing *2*) a weak ON- or OFF-center STA if they are not balanced exactly. We expect that most of such RGCs would be excluded from the analysis by the STA significance requirements (see below), but we cannot exclude the possibility that some of the classified ON and OFF cells might be ON-OFF cells.

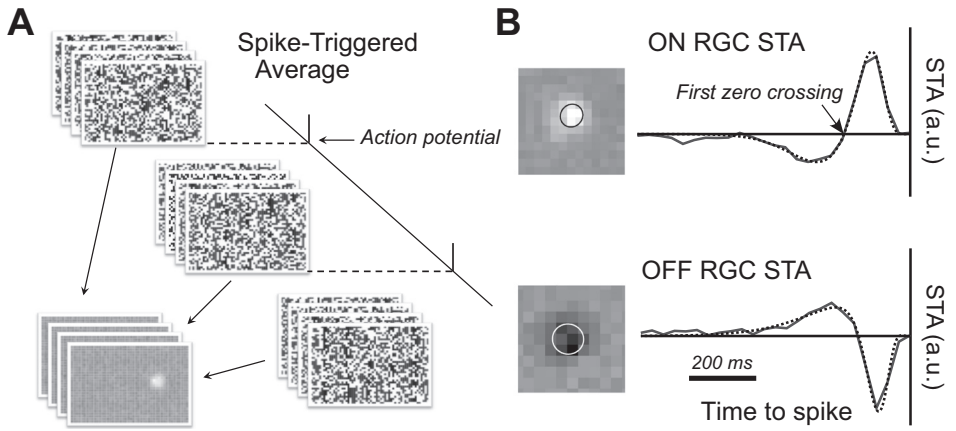

Fig. 2. STA response to binary white noise stimulus. *A*: the STA is the frame-by-frame average of the short spatiotemporal white noise movie that precedes each action potential of an RGC. The spatial sensitivity profile of the RGC (receptive field) corresponds to the STA regions with significant deviation from the average gray level. *B*: visual STAs of the example ON- and OFF-center rat RGCs. For each cell, the STA frame corresponding to the largest deviation from gray level within the receptive field is shown. The spatial extent of the receptive field is quantified by fitting a 2-dimensional Gaussian to this STA frame. An elliptical 1-σ contour of the fit is overlaid on top of the receptive field. The time course shows the STA intensity within the receptive field as a function of time preceding the spike. Overlaid over each time course is a fitted difference of low-pass filters (dotted line). ON and OFF RGCs have opposite signs in the STA deflection preceding the spike. The response latency is estimated as the time to the first zero crossing of the fitted function. a.u., Arbitrary units.

We quantified the response latency of the individual cells by first fitting a difference of two low-pass filters to the time course and then finding the time between the spike and the first fitted time course peak and the time between the spike and the first zero crossing of the time course (Fig. 2*B*). These two time intervals describe dynamics of an RGC response to the light step of the preferred polarity (Chichilnisky and Kalmar 2002). For some cells, the fit to the photovoltaic time course had a small peak before and with opposite polarity with respect to the time course first peak. To avoid using this false peak, we calculated both time to peak and time of the first zero crossing based on the first peak of the fitted function with the deflection polarity matching that of the time course. The mean intensity of some STAs exhibited slight offset from zero. We used the average STA value preceding the spike by 10 to 25 movie frames to determine the offset and subtract it from all of the STA intensities before fitting. The STAs were calculated and parameterized in identical fashion for the visual and photovoltaic responses. RGCs with a time course signal-to-noise (SNR) ratio below 3 were excluded from the analysis. In each preparation, 30% to 60% of the initially identified cells were excluded by this requirement before other cuts described above. For the SNR calculation, the peak value of the time course was used as a signal, and the root mean square value of the 10 time course values most removed from the time of the action potential was used as noise.

Ganglion cell body location. Electrodes with the largest EI signal are located close to the soma and can be used to estimate its position (Li et al. 2015). We estimated the RGC soma location as the center of the two-dimensional Gaussian function fitted to the EI of the cell. The fit location was determined mostly by the somatic signal, which typically had an order of magnitude larger amplitude than the axonal signals. The estimated location of the cell body was then transformed in the stimulus coordinate system for comparison to the location of its receptive field. The transformation was obtained by imaging the known stimulus pattern projected onto the retina at the end of the experiment. Such images capture simultaneously the stimulus pattern and the MEA electrodes, providing the relative angle between RF and EI coordinates. We calculated the center of mass (centroid) location of the receptive fields in the preparation and their average distance from this centroid. The calculations were repeated for the EIs of the same RGCs. The relative shift and scaling between the stimulus and EI coordinates were obtained by matching the centroid locations and average distances from centroid calculated for the receptive fields and EIs. For healthy retinas, we also compared the relative positions of prosthetic and visual receptive field centers by mapping both stimuli coordinates to the same EI coordinate system.

RESULTS

RGCs can respond to complex spatiotemporal patterns at high stimulation frequencies. We characterized the responses of RGCs to complex visual stimuli in seven degenerate (RCS) retinas by activating the subretinally placed photovoltaic array with a binary white noise movie at 20-Hz frame rate. The movie had 70-μm hexagonal pixels, which were aligned with the hexagonal photodiode pixels of the implant (see METHODS).

For 104 RGCs from 7 retinas, the spike-triggered analysis of the white noise stimulus yielded statistically significant responses, with SNR of at least 3 (see METHODS), indicating that the implant successfully elicited RGC responses despite the rapidly varying spatiotemporal structure of the stimulus (Fig. 3). The photovoltaic spike-triggered averages (pSTAs) are the prosthetic equivalent of the classical visual spike-triggered averages (vSTAs), which approximate the temporal characteristics and spatial localization of the RGC receptive fields (Chichilnisky 2001) (Fig. 2). The pSTAs were spatially localized. Seventy-two RGCs had photovoltaic ON (pON) responses with the positive pSTA value of the first peak preceding the spike (see METHODS); 32 RGCs had pOFF responses with the negative time course peak. Two example cells with the distinct pON and pOFF pSTAs are shown in Fig. 3, *A* and *B*, respectively. The pSTAs were similar within a single preparation, although the relative number of cells with pON and pOFF response properties varied between retinal preparations (Fig. 3*C*). The presence of both pON and pOFF responses in the degenerated retina is surprising, given that both ON and OFF bipolar cells are expected to be depolarized by the stimuli and hence provide pON response but no pOFF responses. The observed pOFF responses might be caused by depolarization of the rod bipolar cells that, in turn, relay their excitation through AII amacrine cell to the ON and OFF RGCs (see DISCUSSION for more details). The average receptive field diameter in RCS retina was 195 $\pm$ 6 μm (mean $\pm$ SE) for pON and 170 $\pm$ 8

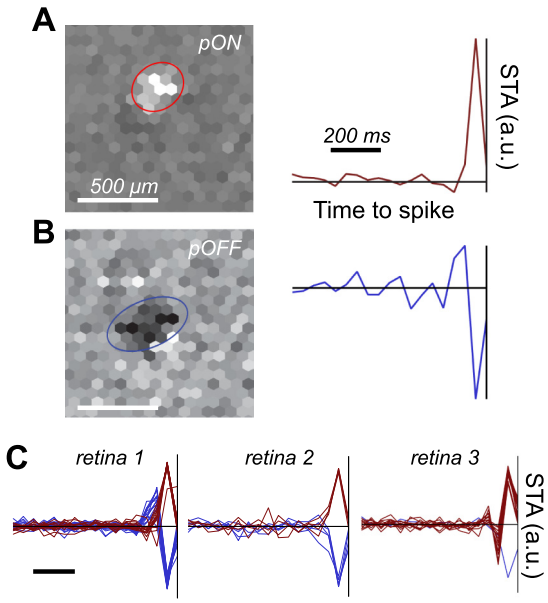

Fig. 3. Photovoltaic spatiotemporal response properties of the RGCs in RCS retinas. *A* and *B*: photovoltaic responses of an example photovoltaic ON (pON) and OFF (pOFF) RGC in RCS retina, respectively. *Left* panels show the receptive field, and *right* panels show the corresponding STA time course. *C*: overlaid time courses of all of the RGCs detected in three separate retinal preparations.

μm for pOFF RGCs, in line with the values previously reported in the literature for low-frequency sparse binary white noise stimulation of the rat retina (Lorach et al. 2015b). We estimated the average response latency by measuring the time between the spike and the first peak and the first zero crossing of the pSTA time course that preceded it (see METHODS). In the linear-nonlinear model of RGCs, the time of the first peak corresponds to the time of maximum rate of increase in the spike frequency in response to the light step of preferred polarity (increase in light level for an ON and decrease for an OFF RGC). In turn, the first zero crossing corresponds to the moment of the maximum response (Chichilnisky and Kalmar 2002). On average, across 7 RCS retinas, the time to first peak was 51 $\pm$ 3 ms for pON and 50 $\pm$ 8 ms for pOFF RGCs. The time to first zero was measured to be 87 $\pm$ 3 ms for pON and 92 $\pm$ 3 ms for pOFF RGCs.

In healthy retina, polarity of the ON and OFF RGC responses to photovoltaic activation is reversed compared with visual stimulation. To compare RGC responses to photovoltaic and visual stimulation in healthy retina, we applied both the visual and photovoltaic white noise stimuli to each LE retinal preparation. The photovoltaic stimulus was identical to the one used in RCS rats. The visual white noise had 60-μm-size square pixels and was refreshed at a 30-Hz frame rate (see METHODS). vSTAs and pSTAs were obtained by reverse correlation analysis between the RGC spike trains we recorded and the stimuli delivered to the retina (Fig. 4). Average response latency, estimated from the STA time courses, was shorter for photovoltaic than for visual stimulation (71 $\pm$ 2 vs. 168 $\pm$ 3 ms, respectively). The faster response to photovoltaic stimulation is likely due to bypassing the phototransduction cascade of normal vision and is consistent with observations previously reported in the literature (Chichilnisky and Kalmar 2002; Mathieson et al. 2012). The average photovoltaic receptive field diameter was 194 $\pm$ 3 μm, compared with 221 $\pm$ 4 μm for the visual receptive fields of the same RGCs (Table 1).

We classified RGCs on the basis of their vSTAs into ON- and OFF-center types (Fig. 4, *A* and *B*, respectively). Using the unique electrophysiological images (EIs) of the RGCs (Li et al. 2015; Petrusca et al. 2007), we matched cells between the visual and prosthetic stimuli (see METHODS). We identified 139 RGCs across 4 preparations that had visual and photovoltaic responses. Polarity of the photovoltaic RGC responses was reversed relative to the visual ones; i.e., visual ON (vON) RGCs behaved as photovoltaic OFF (pOFF), and vOFF RGCs behaved as pON cells (Fig. 4, *A* and *B*). All of the RGCs that had both visual and photovoltaic STA responses in the four LE retinas exhibited this reversal. Although some of the RCS time courses had triphasic shapes (Fig. 3*C*), this feature was more pronounced in LE photovoltaic time courses (Fig. 4*C*).

A possible source of this reversal is the opposite response of photoreceptors to electrical and light stimuli: cells are depolarized by electrical stimulation, but photoreceptors hyperpolarize when illuminated by light. Depolarization of photoreceptors normally corresponds to a decrease in illumination, and hence the retina interprets electrical activation of the photoreceptors as a decrease in light intensity. Thus an increase in the electrical stimuli mimics a decreasing light level, whereas a decrease in electrical stimulation has the same effect as an increase in the light intensity. Consequently, normal signaling from photoreceptors to the ON and OFF bipolar cells should lead to reversed responses with photovoltaic stimulation: pOFF responses of the vON ganglion cells and pON responses of the vOFF ganglion cells. Note that for this hypothesis to hold, the effect of the direct activation of photoreceptors should overwhelm the direct depolarization of ON bipolar cells, which would mediate pON responses in the vON RGCs.

To test if photoreceptors play a role in the photovoltaic responses of the healthy retina, we used a mixture of a 100 μM concentration of the metabotropic glutamate receptor 6 (mGluR6) receptor antagonist LY-341495 and 150 μM of the mGluR6 agonist L-2-amino-4-phosphonobutyric acid to selectively block synaptic transmission from photoreceptors to ON bipolar cells (Sher and DeVries 2012). We then measured the photovoltaic response properties of the RGCs using full-field steps of +100% or −100% contrast (see METHODS). Before application of the blockers, vON cells responded to negative contrast steps with 0.70 $\pm$ 0.57 spikes per step (mean $\pm$ SD; pOFF response) and to positive contrast steps with 1.26 $\pm$ 0.45 spikes per step (pON response) (Fig. 5*B*). vOFF cells responded to positive contrast steps with 1.73 $\pm$ 1.05 spikes per step and did not respond to negative contrast steps (0.01 $\pm$ 0.05 spikes per step). After application of the blockers, visual responses of the vON RGCs to the visual white noise disappeared (Fig. 5*A*), whereas the responses of the vOFF cells remained largely unchanged. Blocking the signal transmission from photoreceptors to the ON bipolar cells led to the complete disappearance of the pOFF photovoltaic responses initially observed in vON RGCs, consistent with pOFF responses being caused by electrical depolarization of photoreceptors. At the same time, pON responses of the vOFF RGCs remained, with 2.55 $\pm$ 1.21 spikes elicited per positive contrast step (Fig. 5*B*). Although these results are consistent with the photovoltaic response in the healthy retina mediated mostly by photoreceptors, it leaves open the question about the

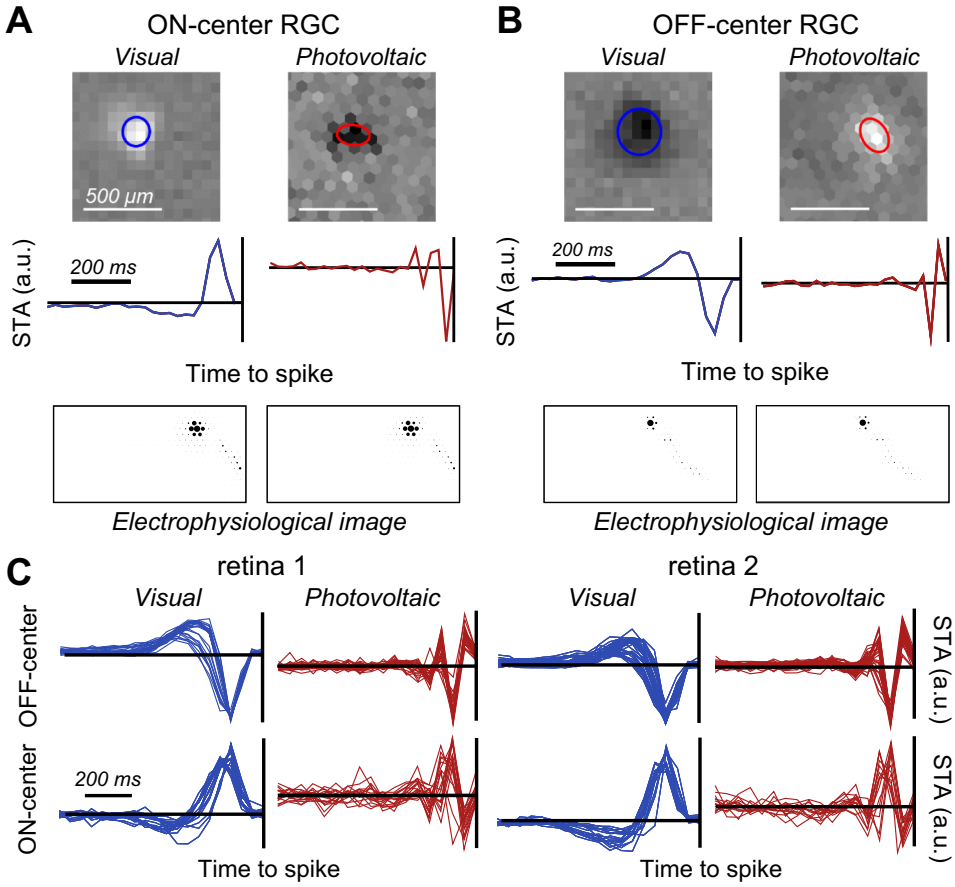

Fig. 4. Visual and photovoltaic spatiotemporal response properties of RGCs in the healthy retina. *A*: responses of an example ON-center RGC. *Top* panels show receptive fields elicited by the visual and photovoltaic stimulation of the same cell, and *middle* panels show the corresponding STA time courses. Polarity of the photovoltaic response is opposite to that of the visual response: the visual ON cell (vON) becomes a photovoltaic OFF cell (pOFF). *Bottom* panels show the identical electrophysiological images of RGCs responding to visual and electrical activation (see METHODS), confirming that the responses of the same RGC were measured. Ellipses overlaid on the receptive fields correspond to the 1-σ contours of the 2-dimensional Gaussians fitted to the receptive fields. *B*: responses of an example OFF-center RGC. The response polarity is again reversed, with the vOFF becoming the pON RGC. *C*: overlaid time courses of all of the RGCs detected in 2 separate retinal preparations. In each preparation the RGCs were divided into vON and vOFF types according to their visual responses (blue traces at *left*). The photovoltaic responses of the same cells (red traces at *right*) show response polarity reversal.

contribution of the direct depolarization of bipolar cell. We did not detect pON responses of the vON RGCs after adding the blockers. However, we cannot say if this was due to such response being negligible or to the ON bipolar cells being driven to the state of constant depolarization or hyperpolarization by the combination of the mGluR6 agonist and antagonist used.

An opposing surround is present in photovoltaic responses. The center-surround organization of the RGC receptive fields is one of the fundamental properties of vision (Kuffler 1953). The classical surround mechanism in the healthy retina is associated with negative feedback by the horizontal cells on the photoreceptor terminals (McMahon et al. 2004; Werblin and Dowling 1969). Inhibitory signaling from amacrine cells in the inner retina is another source of an opposing surround (Flores-Herr et al. 2001; Ichinose and Lukasiewicz 2005; Taylor 1999). We investigated whether the antagonistic surround is maintained under electrical stimulation, because disappearance of photoreceptors and their terminals in retinal degeneration is likely to eliminate the role of horizontal cells, and it is not clear how the electrical surround is affected by the associated retinal rewiring (Jones and Marc 2005).

Table 1. *Comparison of the spatiotemporal characteristics of the visual and photovoltaic responses*

	RCS pON	RCS pOFF	LE pON	LE pOFF	LE vON	LE vOFF
Cell count	72	32	93	46	46	93
RF diameter, μm	195 ± 6	170 ± 8	203 ± 3	177 ± 4	202 ± 5	230 ± 4
Response latency/time to zero, ms	94 ± 5	90 ± 8	76 ± 2	63 ± 2	185 ± 4	160 ± 2
Time to first peak, ms	50 ± 3	56 ± 3	55 ± 2	42 ± 3	109 ± 2	98 ± 1
Distance between EI and RF centers, μm	52 ± 5 (n = 35)	81 ± 17 (n = 10)	79 ± 4 (n = 115)		53 ± 4 (n = 115)	
Distance between photovoltaic and visual RF centers, μm			63 ± 5 (to vOFF) (n = 76)	72 ± 6 (to vON) (n = 39)	72 ± 6 (to pOFF) (n = 39)	63 ± 5 (to pON) (n = 76)

Data are means ± SE; some averages were calculated for a subset of the cells, and cell counts for those measurements are shown separately. Cell counts indicate the number of identified cells that exhibited visual and/or photovoltaic responses and were used in the calculation of the averages. Receptive field (RF) diameter represents the average STA RF sizes for visual and photovoltaic responses. Average response latency (time to zero crossing) was estimated from the photovoltaic and visual STA time courses. Average time to first peak was estimated from the photovoltaic and visual STA time courses. Distance between the electrophysiological images (EI) and RF centers indicates the offsets between RF center location and cell soma, whereas distance between photovoltaic and visual RF centers indicates the offsets between photovoltaic and visual RF center locations. See METHODS section for a description of how the quantities shown were calculated.

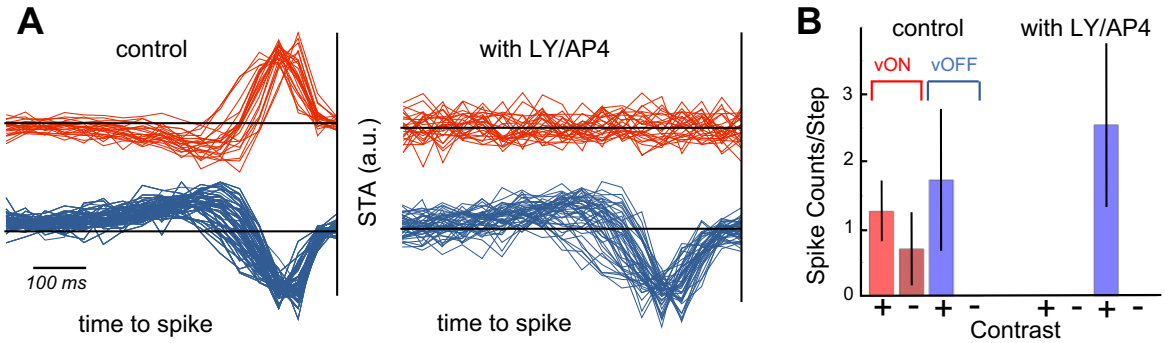

Fig. 5. Effect of blockers on RGC responses. *A*: STA time courses of RGCs with and without blockers (LY, LY-341495; AP4, L-2-amino-4-phosphonobutyric acid). pON responses completely disappeared under the influence of blockers, whereas pOFF cells remained active. *B*: spike counts of cells responding to ±100% contrast steps. The sign of the step is indicated on the horizontal axis with + for positive and – for negative contrast steps. Error bars correspond to SD.

To test if an opposing surround is present in photovoltaic responses, we measured the surround and central signals in the following way. The center signal was estimated as the average (per pixel) STA time course for the pixels located within the 2-σ ellipse of the two-dimensional Gaussian fit to the receptive field. The surround signal was calculated as the average STA time course for the pixels located outside the central zone, in the (4–8)σ band for visual and (3–6)σ band for the photovoltaic STAs. The cutoff values were selected so as to avoid the region where the center signal switches to the surround while maximizing both center and surround signals. As expected, we observed opposing surround signals in both vON and vOFF vSTAs. Figure 6, *A* and *B*, shows two example RGCs with visual surrounds having opposite stimulus preference (sign of the time course deflection preceding a spike) compared with their centers. With electrical stimulation of the same cells, we observed reversal of the polarity not only in centers but also in the antagonistic surround in the LE pSTAs (Fig. 6, *C* vs. *A* and *D* vs. *B*). Surprisingly, the photovoltaic responses of the RGCs in the degenerate RCS retina also had opposing surround signals (Fig. 6, *E* and *F*).

We quantified the strength and sign of the center and surround by measuring the maximum time course deflection preceding the spike. Spatial properties of the center and surround signals were characterized by calculating the STA response as a function of distance from the receptive field center. Figure 6*G* shows that both visual and photovoltaic STAs have opposing surrounds that are wider than the center and become weaker with increasing distance. Photovoltaic surrounds were stronger than visual ones, except for the RCS pOFF RGCs, as measured by the ratio of the maximum surround amplitude to that of the center (Fig. 6*G*). We noticed that cell-to-cell variability of the surround signal was larger for the LE pOFF RGCs than for the other responses. A possible explanation is that direct stimulation of the bipolar cells and photoreceptors has opposite effects on the pOFF RGCs. The balance between these two mechanisms determines the strength of the response, leading to larger cell-to-cell variability than in the pON RGCs in LE and RCS retinas, for which both photoreceptor-mediated and bipolar cell-mediated stimulation mechanisms affect the cell in the same way.

Subretinal electrical stimulation preserves the retinotopic mapping. Retinotopic mapping between the input patterns and RGC somata is essential for proper image formation in the brain. If retinotopic mapping is not preserved in prosthetic vision, stimulation patterns can appear distorted to a patient, as in the case of axonal activation by epiretinal prostheses (Nanduri et al. 2012; Weitz et al. 2015). As shown above, the photovoltaic responses of the ganglion cells to high-frequency binary white noise were spatially localized, with receptive field sizes similar to those obtained with visible light stimulation (Table 1). These results also matched receptive field sizes previously reported using low-frequency sparse white noise stimuli (Lorach et al. 2015b).

We verified proximity between the receptive field center and the RGC soma by measuring the distance between the center of the functional receptive field and the RGC cell body location estimated from its EI (see METHODS). The average displacement between the center of the receptive field and cell soma in photovoltaic stimulation of the RCS retina was 52 ± 5 and 81 ± 17 μm for pON and pOFF RGCs, respectively (Table 1). The average displacement between visual receptive fields and cell somas in the healthy retina was measured to be 53 ± 4 μm. Finally, the average displacement between visual and prosthetic receptive field centers was 68 ± 8 μm, with no significant difference between the cell types. Directions of the individual RGCs displacements were random. All displacements were smaller than the corresponding receptive field sizes. Together with spatially localized STAs, these results suggest that retinotopic mapping is preserved in the degenerate retina.

DISCUSSION

Preservation of the spatiotemporal response properties of individual RGCs in prosthetic vision is important for successful restoration of sight to patients blinded by retinal degeneration. Natural vision relies on multiple parallel pathways in the retina, each corresponding to its own RGC type. Whereas each of these pathways has its unique spatiotemporal and sometimes chromatic response properties, the following three features have been found to be almost universal among different types of the RGCs: *1*) fast (fraction of a second) response, *2*) spatially localized receptive fields, and *3*) antagonistic center-surround organization of the receptive fields.

We found that RGCs in both healthy and degenerate retinas respond to photovoltaic spatiotemporal binary white noise at 20-Hz frame rate. The spatial localization of the response is preserved by subretinal photovoltaic stimulation. At the same time, the response is significantly faster. Antagonistic center-surround organization of the photovoltaic receptive fields is

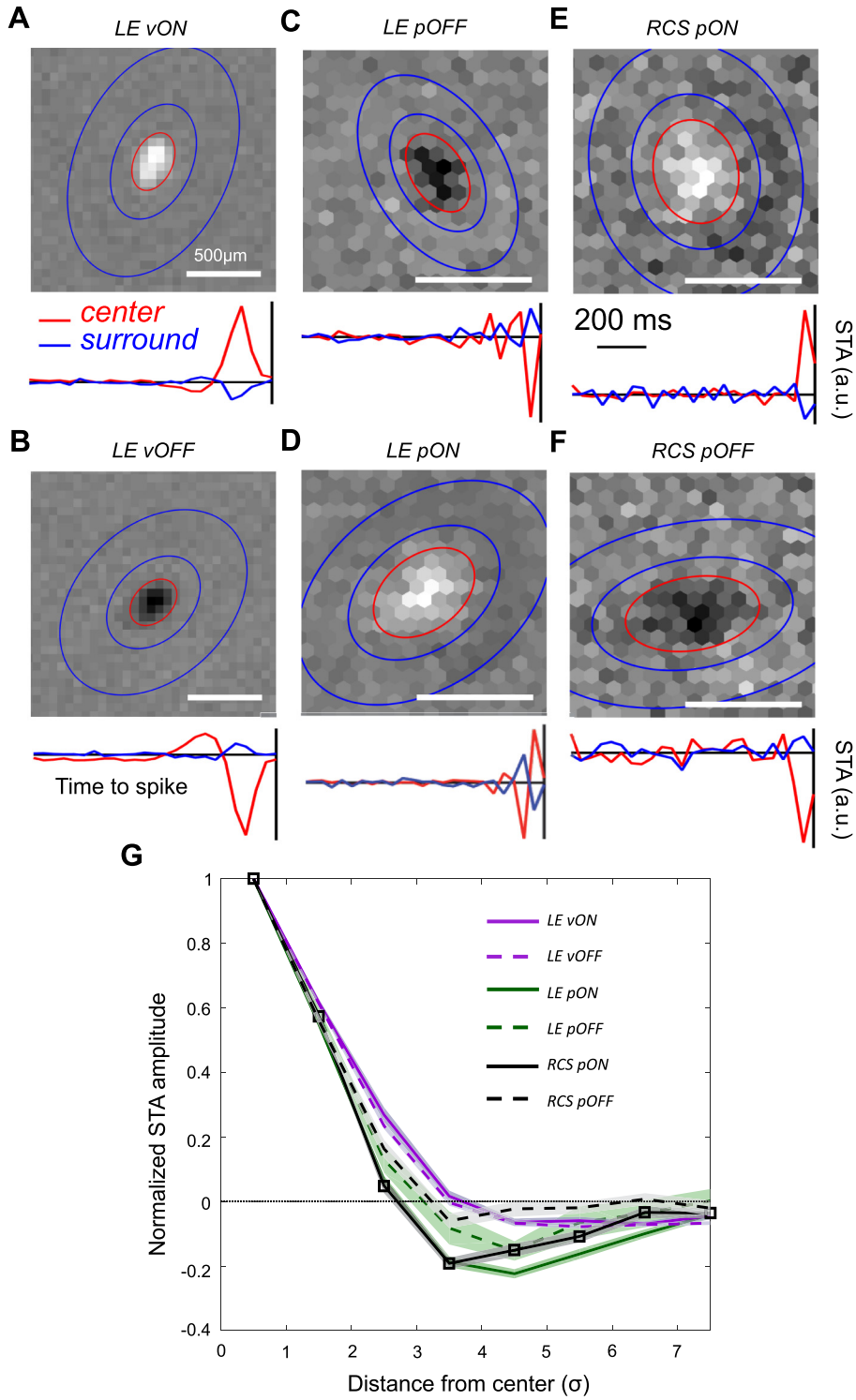

Fig. 6. Center-surround organization of the receptive fields. *A*: the visual STA receptive field of an ON RGC in the healthy LE retina (*top*). The center and surround time courses are shown at *bottom*. The center time course is calculated as the average time course of the pixels located inside the red ellipse. The surround time course is the average of the pixels located between the 2 blue ellipses. *B–F* show receptive fields as well as the center and surround time courses calculated in the same way for visual response of a vOFF LE RGC and photovoltaic response of an example LE pOFF, LE pON, RCS pON, and RCS pOFF RGC, respectively. *G*: STA response (peak time course deflection preceding the spike) vs. distance from the center of the receptive field. The curves represent the average responses of all the identified RGCs. The distance from the center was measured in standard deviations of the 2-dimensional Gaussian fitted to the STA receptive field. The average time course deflections were calculated for eight 1-σ wide bins. The average deflections in each bin were normalized to the deflection in the most central bin. The markers on the RCS pON response curve show centers of the bins. The bands correspond to the SE. Visual and photovoltaic OFF responses were inverted for the ease of comparison.

present in both healthy and degenerated retinas. Photovoltaic stimulation in healthy retina leads to distinct responses of the ON- and OFF-center RGCs, opposite to their responses to visual stimulation. Both pON and pOFF STAs are present in degenerated retina, although it is not clear which RGC types exhibit these distinct responses. These findings and their implications are discussed below.

It has been shown previously that spatially simple (full-field or 1-dimensional reversing gratings) and temporally slow (2 Hz) amplitude modulation of high-frequency (20 to 40 Hz) trains of subretinal photovoltaic pulses resulted in transient responses of the RGCs to slow changes in light intensity (Goetz et al. 2015; Lorach et al. 2015b). These results indicated that subretinal photovoltaic stimulation preserves flicker fusion and adaptation to static images. It was also reported that retinal network-mediated responses can be elicited by epiretinal stimulation at 25 Hz with static spatial distribution but stochastic temporal changes in amplitude, indicating that fast changes in

the full-field stimulation can elicit responses despite the flicker fusion (Sekhar et al. 2016).

In this study, we have demonstrated for the first time that retina responds to spatiotemporal white noise stimulation delivered through a photovoltaic subretinal prosthesis at 20-Hz frame rate. Retinal response to complex spatial and fast temporal patterns exhibited many similarities to natural visual response.

Spatiotemporal properties of the response to photovoltaic stimulus. Localized RGC receptive fields are essential for the transmission of spatial information to the brain. We observed that the size of the receptive fields was similar between photovoltaic and visual responses in the healthy retina. This size did not increase in the degenerate retina, which is consistent with our previous results obtained with a slow (2 Hz) sparse white noise stimulus, where a single random pixel was illuminated in each frame (Lorach et al. 2015b). Our current measurements demonstrate that spatial localization is preserved in response to a more dynamic and complex stimulus. Furthermore, we have shown that the photovoltaic receptive fields of individual RGCs colocalize with their cell bodies, thereby preserving the topological mapping between the inputs into the retina and their representation in the brain. This is an important feature of the network-mediated retinal responses achieved by subretinal implants. Epiretinal implants have been shown to disturb this mapping due to direct activation of axons from remote neurons, which results in distorted visual percepts (Nanduri et al. 2012; Weitz et al. 2015).

Temporal response properties of the RGCs, as measured through the STA time course, confirm that the photovoltaic response has shorter latency than the visual one (Mandel et al. 2013; Mathieson et al. 2012), most likely because it bypasses the phototransduction cascade in the photoreceptors. Latency of the photovoltaic responses in healthy retina was somewhat shorter than in the degenerated retina (Table 1). Changes in the neural circuitry of the degenerated retina do not allow for a clear interpretation of this difference. Both the photovoltaic and visual STA time courses had no significant deflection from the average gray level up until about a few hundred milliseconds before the spike. This suggests that RGC spiking activity is affected only by the most recent changes in the stimulus. Such short "memory" is another essential feature of prosthetic vision enabling responses to a rapidly changing visual stimulus. It is important to note that uncertainties of the response latencies in Table 1 are purely statistical. They were calculated on the basis of the cell-to-cell variability of the responses. Additional uncertainty comes from the low sampling rate of the photovoltaic response measurement. The 20-Hz photovoltaic white noise movie allowed for 50-ms sampling of the time course, likely resulting in overestimation of the latencies. Thus, although we can state with certainty that the photovoltaic responses have shorter latencies than the visual ones, the reported values of these latencies should be used as estimates of the maximum, rather than the exact values.

One distinct feature of the photovoltaic STA was three, and sometimes four or five (Figs. 3, 4, and 6), peaks in the time course, whereas visual time courses most often have only two peaks. The STA convolution with the stimulus predicts the linear portion of the RGC response in a linear-nonlinear (LN) model of the retina (Chichilnisky 2001). Therefore, the first peak before the spike determines the sign of the preferred change of light level. The second peak of the opposite sign, in turn, predicts how transient the response of the cell will be to a light step of the preferred polarity (Chichilnisky and Kalmar 2002). Thus the LN model predicts that the spike rate of the RGC will increase and then decrease in response to the preferred direction of the light level change. More than two peaks suggest that RGC will increase and decrease its spike rate more than once in response to the same stimulus. One possible explanation is that flicker fusion does not happen instantaneously and that the response to the change in the NIR pulse amplitude persists for a few pulses following the change. With the pulse frequency matching the white noise movie frame rate (20 Hz), such persistence might explain the multiple peaks we observed in the pSTA time course. Increasing the frequency of the NIR pulses might eliminate this effect, and previous studies showed that frequencies as high as 40 Hz can be used (Lorach et al. 2015b). Another possible explanation to multiple peaks could be that they represent the sum of the distinct contributions from the bipolar cells and photoreceptors, which occur at different latencies (Boinagrov et al. 2014).

The opposing center-surround organization we observed in the photovoltaic receptive fields of RGCs in the healthy and in degenerate retinas is another important feature of retinal signal processing preserved in prosthetic vision. Our result is corroborated by the recent study reporting opposing surround in the degenerated mouse retina in response to a subretinal electric stimulation (Stutzki et al. 2016). Receptive field surrounds are thought to contribute to edge detection, and their preservation might result in better prosthetic vision. Two mechanisms are thought to be responsible for the opposing wide surrounds in the visual receptive fields of the healthy retina: *1*) negative feedback onto the photoreceptors by the network of the horizontal cells (McMahon et al. 2004; Werblin and Dowling 1969) and *2*) amacrine cells providing inhibitory inputs to bipolar and ganglion cells (Cook et al. 1998; Flores-Herr et al. 2001; Ichinose and Lukasiewicz 2005; Taylor 1999). Absence of photoreceptors in the degenerate retina eliminates the original contribution of the horizontal cells to the surround in the RCS retina. At the same time, the surviving horizontal cells form synapses in the inner plexiform layer (Jones and Marc 2005), and we cannot eliminate a possibility of their contribution to the observed surround. Amacrine cells survive the degeneration process (Jones and Marc 2005; Marc and Jones 2003) and can provide the opposing surround, as well. Determination of the balance between the two mechanisms will require further studies. Both mechanisms involve the surround signal crossing at least one additional synapse compared with the center signal. We see that the surround signals were indeed somewhat delayed in the visual responses. The surround time course had the first peak occur earlier than the center, relative to the spike (Fig. 6, *A* and *B*). The coarser time resolution of the 20-Hz frame rate, compared with 30 Hz in the visual stimulus, did not allow us to accurately measure this difference in the photovoltaic time courses (Fig. 6, *C–F*). Intensity of the surround relative to the center in photovoltaic receptive fields was stronger than in the visual responses, except for the RCS pOFF RGCs.

Selective photovoltaic activation of ON and OFF pathways in the healthy retina. The distinctly different responses of the ON- and OFF-center RGCs to photovoltaic stimulation in healthy retina, opposite in polarity of their natural visual

response, is consistent with electrical depolarization of the photoreceptors, which overcomes the effects of the direct bipolar cell stimulation and elicits responses opposite to hyperpolarization of photoreceptors under visible light. This explanation is supported by elimination of the photovoltaic OFF responses on pharmacological blockade of neural transmission from photoreceptors to ON bipolar cells. Our results are consistent with previous findings that ON and OFF RGCs in healthy rabbit retina can be activated by the opposite phases of a sinusoidal electrical stimulus, and that the response of the ON RGCs disappears when the photoreceptor to ON bipolar cells transmission is selectively blocked (Freeman and Fried 2011). It was also shown in the healthy mouse retina that the network-mediated component of ON and OFF RGC responses to temporal Gaussian electrical white noise, delivered epiretinally, have distinct STA time courses (Sekhar et al. 2017). As a result, it becomes clear that electrical stimulation of the healthy retina preserves the two major retinal pathways, only operating in reversed polarity: ON becoming OFF, and vice versa, compared with visual responses.

Distinct pON and pOFF responses in the degenerated retina. Presence of the distinctly different pON and pOFF responses in the degenerated retina is intriguing. In the absence of photoreceptors, direct depolarization of the bipolar cells with "feedforward" excitatory signaling to the RGCs should result in all of the RGCs having pON response properties. One possible mechanism for introducing the two response polarities is the depolarization of the rod bipolar cells. In the healthy retina, rod bipolar cells relate their signals to the cone pathway through AII amacrine cells that have the sign-inverting glycinergic synapse with the OFF cone pathway and the sign-preserving gap-junction coupling to the ON cone pathway. If this circuitry were preserved in the degenerated retina, direct depolarization of rod bipolar cells and/or the AII amacrine cells by the photovoltaic prosthesis would lead to the visual ON RGCs being excited at the onset of the photovoltaic stimulus and exhibiting pON responses. In turn, the visual OFF RGCs would have inhibition removed from them at the end of the photovoltaic stimulation and exhibit pOFF response properties. This hypothesis assumes that the consequences of the direct depolarization of the cone ON and OFF bipolar cells are overwhelmed by the signals from the rod pathway. In absence of visual responses in the RCS retina, we could not verify the predicted identity of the RGCs with pON and pOFF response properties. Although the presence of the pOFF responses in the degenerating retina is surprising, it was also recently observed in the RGC responses to temporal Gaussian electrical white noise, delivered epiretinally to the degenerate mouse retina (Sekhar et al. 2017).

An alternative explanation is that some photoreceptor cells survive degeneration and that the pON and pOFF responses are mediated through them, similarly to the LE retina. LE rat retina has about eight layers of photoreceptor nuclei. In RCS rat, by p90, at most a single layer of photoreceptor nuclei is left, and by p180, practically all photoreceptors are gone (Sauvé et al. 2001). Our experiments were performed in rats aged p120 to p360, so we cannot exclude the possibility that some photoreceptor cell bodies were still present in the younger animals. However, we did not observe a significant trend in the number of responsive cells or in the ratio between detected pON and pOFF cells over this big range of the degeneration progression. This leads us to believe that the few remaining photoreceptors were not the main conduit of the RGC responses in degenerate retina.

Implications of the pON and pOFF responses. Selectivity of the pON and pOFF responses present in the healthy retina might disappear after complete photoreceptor degeneration and therefore might be useful only during the limited period when patients lose outer segments, but the photoreceptor nuclei are still present. However, even in this case, subretinal implants block the supply of nutrients from the choroid to the retina, which quickly eliminates the remaining photoreceptor somas (Lorach et al. 2015a, 2015b; 2015c; Mandel et al. 2013). Epiretinal implants do not have such an effect. Long ($\geq$25 ms) electrical pulses delivered by an epiretinal implant have been shown to elicit selective network responses (Weitz et al. 2015). If stimulation of photoreceptors without activation of the RGCs and bipolar cells were possible, it could take advantage of the selective activation of the ON and OFF retinal pathways while some photoreceptor somas are still present in degenerating retina.

Implications of the distinct pON and pOFF responses in degenerated retina are less certain because the identity of the RGCs exhibiting these responses is yet unknown. If our hypothesis regarding rod bipolar cell-mediated responses is correct, selective activation of the ON and OFF pathways might be possible. However, scarcity of the rod bipolar cells in the center of the macula would prevent the proposed mechanism from being utilized in the foveal region.

Conclusions. Our measurements show that spatiotemporal properties of the RGC receptive fields in photovoltaic network-mediated stimulation of the degenerate retina are similar to those of natural vision, with the most pronounced difference being shorter latency of the photovoltaic responses. Both types of responses are spatially localized, have fast dynamics, and exhibit opposing center-surround organization. Furthermore, we show that not only ON but also OFF responses to prosthetic stimulation are possible. These similarities raise confidence that subretinal stimulation via small photovoltaic pixels with local return electrodes can result in functional prosthetic vision.

ACKNOWLEDGMENTS

We thank James Harris for his role in fabrication of the photovoltaic arrays, and Sergei Kachiguine and Alan Litke for providing access to and maintaining the multielectrode array recording system.

GRANTS

Support was provided by National Eye Institute Grant R01 EY-018608 (to D. Palanker), Department of Defense Grant W81XWH-15-1-0009 (to D. Palanker), the Stanford Spectrum fund (to D. Palanker), a Stanford Neurosciences Institute Interdisciplinary Award (to G. Goetz), the Pew Charitable Trusts Scholarships in the Biomedical Sciences (to A. Sher), and the SU^2 Program (to K. Mathieson).

DISCLOSURES

Patents of D. Palanker related to photovoltaic restoration of sight are licensed by Stanford University to Pixium Vision. D. Palanker is a consultant to Pixium Vision. Other authors declare no financial interests.

AUTHOR CONTRIBUTIONS

D.P. and A.S. conceived and designed research; E.H. and R.S. performed experiments; E.H., R.S., and A.S. analyzed data; E.H., R.S., G.G., D.P., and

A.S. interpreted results of experiments; E.H., R.S., G.G., and A.S. prepared figures; E.H., R.S., G.G., D.P., and A.S. drafted manuscript; E.H., R.S., G.G., K.M., D.P., and A.S. edited and revised manuscript; E.H., R.S., G.G., X.L., L.G., T.I.K., J.H., K.M., D.P., and A.S. approved final version of manuscript.

REFERENCES

Boinagrov D, Lei X, Goetz G, Kamins T, Mathieson K, Galambos L, Harris J, Palanker DV. Photovoltaic pixels for neural stimulation: circuit models and performance. *IEEE Trans Biomed Circuits Syst* 10: 85–97, 2016. doi:10.1109/TBCAS.2014.2376528.

Boinagrov D, Pangratz-Fuehrer S, Goetz G, Palanker D. Selectivity of direct and network-mediated stimulation of the retinal ganglion cells with epi-, sub- and intraretinal electrodes. *J Neural Eng* 11: 026008, 2014. doi:10.1088/1741-2560/11/2/026008.

Chander D, Chichilnisky EJ. Adaptation to temporal contrast in primate and salamander retina. *J Neurosci* 21: 9904–9916, 2001.

Chichilnisky EJ. A simple white noise analysis of neuronal light responses. *Network* 12: 199–213, 2001. doi:10.1080/713663221.

Chichilnisky EJ, Kalmar RS. Functional asymmetries in ON and OFF ganglion cells of primate retina. *J Neurosci* 22: 2737–2747, 2002.

Cook PB, Lukasiewicz PD, McReynolds JS. Action potentials are required for the lateral transmission of glycinergic transient inhibition in the amphibian retina. *J Neurosci* 18: 2301–2308, 1998.

Devries SH, Baylor DA. Mosaic arrangement of ganglion cell receptive fields in rabbit retina. *J Neurophysiol* 78: 2048–2060, 1997. doi:10.1152/jn.1997.78.4.2048.

Field GD, Gauthier JL, Sher A, Greschner M, Machado TA, Jepson LH, Shlens J, Gunning DE, Mathieson K, Dabrowski W, Paninski L, Litke AM, Chichilnisky EJ. Functional connectivity in the retina at the resolution of photoreceptors. *Nature* 467: 673–677, 2010. doi:10.1038/nature09424.

Field GD, Sher A, Gauthier JL, Greschner M, Shlens J, Litke AM, Chichilnisky EJ. Spatial properties and functional organization of small bistratified ganglion cells in primate retina. *J Neurosci* 27: 13261–13272, 2007. doi:10.1523/JNEUROSCI.3437-07.2007.

Flores-Herr N, Protti DA, Wässle H. Synaptic currents generating the inhibitory surround of ganglion cells in the mammalian retina. *J Neurosci* 21: 4852–4863, 2001.

Freeman DK, Eddington DK, Rizzo JF III, Fried SI. Selective activation of neuronal targets with sinusoidal electric stimulation. *J Neurophysiol* 104: 2778–2791, 2010. doi:10.1152/jn.00551.2010.

Freeman DK, Fried SI. Multiple components of ganglion cell desensitization in response to prosthetic stimulation. *J Neural Eng* 8: 016008, 2011. doi:10.1088/1741-2560/8/1/016008.

Goetz G, Smith R, Lei X, Galambos L, Kamins T, Mathieson K, Sher A, Palanker D. Contrast sensitivity with a subretinal prosthesis and implications for efficient delivery of visual information. *Invest Ophthalmol Vis Sci* 56: 7186–7194, 2015. doi:10.1167/iovs.15-17566.

Goetz GA, Mandel Y, Manivanh R, Palanker DV, Čižmár T. Holographic display system for restoration of sight to the blind. *J Neural Eng* 10: 056021, 2013. doi:10.1088/1741-2560/10/5/056021.

Goetz GA, Palanker DV. Electronic approaches to restoration of sight. *Rep Prog Phys* 79: 096701, 2016. doi:10.1088/0034-4885/79/9/096701.

Ho AC, Humayun MS, Dorn JD, da Cruz L, Dagnelie G, Handa J, Barale PO, Sahel JA, Stanga PE, Hafezi F, Safran AB, Salzmann J, Santos A, Birch D, Spencer R, Cideciyan AV, de Juan E, Duncan JL, Eliott D, Fawzi A, Olmos de Koo LC, Brown GC, Haller JA, Regillo CD, Del Priore LV, Arditi A, Geruschat DR, Greenberg RJ; Argus II Study Group. Long-term results from an epiretinal prosthesis to restore sight to the blind. *Ophthalmology* 122: 1547–1554, 2015. doi:10.1016/j.ophtha.2015.04.032.

Humayun MS, Dorn JD, da Cruz L, Dagnelie G, Sahel JA, Stanga PE, Cideciyan AV, Duncan JL, Eliott D, Filley E, Ho AC, Santos A, Safran AB, Arditi A, Del Priore LV, Greenberg RJ; Argus II Study Group. Interim results from the international trial of Second Sight's visual prosthesis. *Ophthalmology* 119: 779–788, 2012. doi:10.1016/j.ophtha.2011.09.028.

Ichinose T, Lukasiewicz PD. Inner and outer retinal pathways both contribute to surround inhibition of salamander ganglion cells. *J Physiol* 565: 517–535, 2005. doi:10.1113/jphysiol.2005.083436.

Jones BW, Marc RE. Retinal remodeling during retinal degeneration. *Exp Eye Res* 81: 123–137, 2005. doi:10.1016/j.exer.2005.03.006.

Kuffler SW. Discharge patterns and functional organization of mammalian retina. *J Neurophysiol* 16: 37–68, 1953. 10.1152/jn.1953.16.1.37.

Li PH, Gauthier JL, Schiff M, Sher A, Ahn D, Field GD, Greschner M, Callaway EM, Litke AM, Chichilnisky EJ. Anatomical identification of extracellularly recorded cells in large-scale multielectrode recordings. *J Neurosci* 35: 4663–4675, 2015. doi:10.1523/JNEUROSCI.3675-14.2015.

Litke AM, Bezayiff N, Chichilnisky EJ, Cunningham W, Dabrowski W, Grillo AA, Grivich MI, Grybos P, Hottowy P, Kachiguine S, Kalmar RS, Mathieson K, Petrusca D, Rahman M, Sher A. What does the eye tell the brain? Development of a system for the large-scale recording of retinal output activity. *IEEE Trans Nucl Sci* 51: 1434–1440, 2004. doi:10.1109/TNS.2004.832706.

Lorach H, Goetz G, Mandel Y, Lei X, Kamins TI, Mathieson K, Huie P, Dalal R, Harris JS, Palanker D. Performance of photovoltaic arrays in-vivo and characteristics of prosthetic vision in animals with retinal degeneration. *Vision Res* 111: 142–148, 2015a [Erratum. *Vision Res* 117: 137, 2015]. doi:10.1016/j.visres.2014.09.007.

Lorach H, Goetz G, Smith R, Lei X, Mandel Y, Kamins T, Mathieson K, Huie P, Harris J, Sher A, Palanker D. Photovoltaic restoration of sight with high visual acuity. *Nat Med* 21: 476–482, 2015b. doi:10.1038/nm.3851.

Lorach H, Kung J, Beier C, Mandel Y, Dalal R, Huie P, Wang J, Lee S, Sher A, Jones BW, Palanker D. Development of animal models of local retinal degeneration. *Invest Ophthalmol Vis Sci* 56: 4644–4652, 2015c. doi:10.1167/iovs.14-16011.

Lorach H, Wang J, Lee DY, Dalal R, Huie P, Palanker D. Retinal safety of near infrared radiation in photovoltaic restoration of sight. *Biomed Opt Express* 7: 13–21, 2016. doi:10.1364/BOE.7.000013.

Mandel Y, Goetz G, Lavinsky D, Huie P, Mathieson K, Wang L, Kamins T, Galambos L, Manivanh R, Harris J, Palanker D. Cortical responses elicited by photovoltaic subretinal prostheses exhibit similarities to visually evoked potentials. *Nat Commun* 4: 1980, 2013. doi:10.1038/ncomms2980.

Marc RE, Jones BW. Retinal remodeling in inherited photoreceptor degenerations. *Mol Neurobiol* 28: 139–147, 2003. doi:10.1385/MN:28:2:139.

Mathieson K, Loudin J, Goetz G, Huie P, Wang L, Kamins TI, Galambos L, Smith R, Harris JS, Sher A, Palanker D. Photovoltaic retinal prosthesis with high pixel density. *Nat Photonics* 6: 391–397, 2012. doi:10.1038/nphoton.2012.104.

McMahon MJ, Packer OS, Dacey DM. The classical receptive field surround of primate parasol ganglion cells is mediated primarily by a non-GABAergic pathway. *J Neurosci* 24: 3736–3745, 2004. doi:10.1523/JNEUROSCI.5252-03.2004.

Nanduri D, Fine I, Horsager A, Boynton GM, Humayun MS, Greenberg RJ, Weiland JD. Frequency and amplitude modulation have different effects on the percepts elicited by retinal stimulation. *Invest Ophthalmol Vis Sci* 53: 205–214, 2012. doi:10.1167/iovs.11-8401.

Palanker D, Vankov A, Huie P, Baccus S. Design of a high-resolution optoelectronic retinal prosthesis. *J Neural Eng* 2: S105–S120, 2005. doi:10.1088/1741-2560/2/1/012.

Petrusca D, Grivich MI, Sher A, Field GD, Gauthier JL, Greschner M, Shlens J, Chichilnisky EJ, Litke AM. Identification and characterization of a Y-like primate retinal ganglion cell type. *J Neurosci* 27: 11019–11027, 2007. doi:10.1523/JNEUROSCI.2836-07.2007.

Sauvé Y, Girman SV, Wang S, Lawrence JM, Lund RD. Progressive visual sensitivity loss in the Royal College of Surgeons rat: perimetric study in the superior colliculus. *Neuroscience* 103: 51–63, 2001. doi:10.1016/S0306-4522(00)00557-1.

Sekhar S, Jalligampala A, Zrenner E, Rathbun DL. Tickling the retina: integration of subthreshold electrical pulses can activate retinal neurons. *J Neural Eng* 13: 046004, 2016. doi:10.1088/1741-2560/13/4/046004.

Sekhar S, Jalligampala A, Zrenner E, Rathbun DL. Correspondence between visual and electrical input filters of ON and OFF mouse retinal ganglion cells. *J Neural Eng* 14: 046017, 2017. doi:10.1088/1741-2552/aa722c.

Sher A, DeVries SH. A non-canonical pathway for mammalian blue-green color vision. *Nat Neurosci* 15: 952–953, 2012. doi:10.1038/nn.3127.

Smith W, Assink J, Klein R, Mitchell P, Klaver CC, Klein BE, Hofman A, Jensen S, Wang JJ, de Jong PT. Risk factors for age-related macular degeneration: pooled findings from three continents. *Ophthalmology* 108: 697–704, 2001. doi:10.1016/S0161-6420(00)00580-7.

Stingl K, Bartz-Schmidt KU, Besch D, Braun A, Bruckmann A, Gekeler F, Greppmaier U, Hipp S, Hörtdörfer G, Kernstock C, Koitschev A, Kusnyerik A, Sachs H, Schatz A, Stingl KT, Peters T, Wilhelm B, Zrenner E. Artificial vision with wirelessly powered subretinal electronic implant alpha-IMS. *Proc Biol Sci* 280: 20130077, 2013b. doi:10.1098/rspb.2013.0077.

Stingl K, Bartz-Schmidt K-U, Gekeler F, Kusnyerik A, Sachs H, Zrenner E. Functional outcome in subretinal electronic implants depends on foveal eccentricity. *Invest Ophthalmol Vis Sci* 54: 7658–7665, 2013a. doi:10.1167/iovs.13-12835.

Stutzki H, Helmhold F, Eickenscheidt M, Zeck G. Subretinal electrical stimulation reveals intact network activity in the blind mouse retina. *J Neurophysiol* 116: 1684–1693, 2016. doi:10.1152/jn.01095.2015.

Taylor WR. TTX attenuates surround inhibition in rabbit retinal ganglion cells. *Vis Neurosci* 16: 285–290, 1999. doi:10.1017/S0952523899162096.

Wang L, Mathieson K, Kamins TI, Loudin JD, Galambos L, Goetz G, Sher A, Mandel Y, Huie P, Lavinsky D, Harris JS, Palanker DV. Photovoltaic retinal prosthesis: implant fabrication and performance. *J Neural Eng* 9: 046014, 2012. doi:10.1088/1741-2560/9/4/046014.

Weitz AC, Nanduri D, Behrend MR, Gonzalez-Calle A, Greenberg RJ, Humayun MS, Chow RH, Weiland JD. Improving the spatial resolution of epiretinal implants by increasing stimulus pulse duration. *Sci Transl Med* 7: 318ra203, 2015. doi:10.1126/scitranslmed.aac4877.

Werblin FS, Dowling JE. Organization of the retina of the mudpuppy, *Necturus maculosus*. II. Intracellular recording. *J Neurophysiol* 32: 339–355, 1969.

Yue L, Weiland JD, Roska B, Humayun MS. Retinal stimulation strategies to restore vision: Fundamentals and systems. *Prog Retin Eye Res* 53: 21–47, 2016. doi:10.1016/j.preteyeres.2016.05.002.